NUMERICAL SIMULATION OF HIGH VELOCITY STARS

by

Sudarshan Luitel, B.S.

A thesis submitted to the Graduate College of
Texas State University in partial fulfillment
of the requirements for the degree of
Master of Science
with a Major in Physics
August 2021

Committee Members:

Blagoy Rangelov, Chair

Donald Olson

Andrea Banzatti

FAIR USE AND AUTHOR'S PERMISSION STATEMENT

Fair Use

Duplication Permission

DEDICATION

I dedicate this thesis to my amazing wife for her continuous moral support throughout the research and my parents for their encouragement.

ACKNOWLEDGEMENTS

I want to appreciate all the guidance and sincerely thank my advisor Dr. Rangelov for his unwavering support and mentorship. I want to thank committee members Dr. Olson for helping me proofread this thesis and Dr. Banzatti for his comments and kind words.

TABLE OF CONTENTS

Page

LIST OF TABLES

Table **Page**

LIST OF FIGURES

Figure **Page**

ABSTRACT

The origins of high velocity runaway stars have been of interest since their discovery. To shed some light on this important problem in modern astrophysics, we use rapid binary stellar evolution code. We have simulated hundreds of thousands of massive stars in binaries and track their dynamical evolution. We discuss our findings in this work. We show the results for runaway compact objects and regular stars, and discuss the implications of our results. When available, we compare our simulations with observational data.

1. INTRODUCTION

1.1 History and The Formation of Binary Stars

Most of the stars we see in the night sky are binaries. After the invention of the telescope, astronomers began to record their findings; In 1650, J. B. Riccioli was the first astronomer to discover a visual binary system. Sir William Herschel used the biggest telescope of the time to catalog more than 700 binary stars. Herschel was previously skeptical about the binaries' existence but later conceded that these stars were in fact orbiting each other, which he concluded by observing the stars' movements over many years. His son, John Herschel, continued his work, and beginning in 1838 he spent four years in South Africa observing and cataloging 2100 binary stars (Niemela, 2001).

Stars are born when a formation of "dense protostellar core" begins and a central region of molecular cloud gravitationally collapses. The core evolves into a singular isothermal sphere where the exterior of the protostellar core falls towards the center of the protostellar core (Shu, 1983; Shu et al., 1987). The best understanding we have of binary star formation is that it forms through a continuous fragmentation during molecular cloud collapse; it has been demonstrated using the numerical simulation, which seems to produce a pair of clumps (Boss, 1988). Single star formation is rare and most if not all the stars form with one or more companions (Larson, 2003). Binary formation is considered more stable than a formation of multi stars systems. Moreover, massive stars tend to pair up with another massive star (Sana et al., 2012).

1.2 Types of Binaries

There are four main types of binary systems: visual binary, spectroscopic binary, eclipsing binary, and astrometric binary.

- Visual Binaries: Visual binaries are typically widely separated from each other and we can resolve both stars using a telescope. They are usually relatively close to Earth. Visual binaries are also called orbital binaries because their orbit and masses can be calculated from observation. Only 2200 orbital binary pairs have been catalogued (Malkov and Chulkov, 2017). Most of the visual binaries do not experience mass transfer because their orbital period could extend up to thousands of years. Indeed, numerical simulations shows the mass transfer between binary stars with large separation is not as common as close binaries.

- Spectroscopic Binary: Spectroscopic binaries are close binaries,whose separation is unresolved even with big modern telescopes. We use spectroscopic method to detect the binaries, hence the name spectroscopic binaries. When these binaries orbit each other, we can observe the Doppler shift in the spectral lines, which is used to calculate the radial velocity and the distance between them (Struve and Huang, 1958).

- Eclipsing Binary: Just as the word eclipse suggests, eclipsing binaries are the type where stars eclipse each other in the line of sight. When the eclipse occurs the intensity of the light changes. If the stars are of same mass and temperature, the depth of the peak are the same. More interesting phenomena occur when a cooler star eclipses the hotter star or vice versa. The curve of intensity is deeper when a cooler one is in front of the hotter one and the depth decreases when the hotter star eclipses the cooler one (Southworth, 2012). We use photometry to analyze eclipsing binaries which is done by measuring the intensity of the system over time.

- Astrometric Binary: When the primary star is much more brighter than a companion the secondary blends with the primary star (both stars are too close to each other to be resolved). Observed over time, astrometric binaries show a perturbation or “wobble” in their proper motion, due to the gravitational influence

of an unseen companion. To detect this unresolved system, we look at the tiniest perturbation in the intensity and its effects on the nearby stars or star systems. We use application of the image tube and photoelectric scanning to observe the perturbation (Southworth, 2012).

1.3 Stellar Evolution

Binary stars evolve slightly differently than a single star, but the internal mechanisms of individual stars are governed by the same physical laws. Individual stars in a binary system go through same stellar evolution process as single stars.

Stars in the main sequence (Figure 1.1) fuse hydrogen into helium in their cores. Mass of the main sequence ranges from $\sim 0.1\,\mathrm{M}_{\odot}$ to $\sim$200 $\mathrm{M}_{\odot}$; our Sun, for example, is a main-sequence star. Hydrogen fusion in the main sequence increases as the mass increases. Massive stars (>8 $\mathrm{M}_{\odot}$) have a higher fuel supply which increases the rate at which stars burn their fuel. The rate of nuclear fuel combustion can be described by mass-luminosity relation observed in binary stars is given by Eqns. 1.1 and 1.2.

$$L \propto M^{3.5} \tag{1.1}$$

$$t = \frac{M}{L} = \frac{1}{M^{2.5}} \tag{1.2}$$

where L is the luminosity, t is time, and M is the mass of the star. The more massive the star, the more luminous it gets, and the faster it burns its fuel. As a star burns its hydrogen-rich core, it gets brighter and brighter and eventually exhausts its fuel. Once the core can no longer exert pressure to sustain its gravity, hydrostatic equilibrium (Eqn. 1.3)

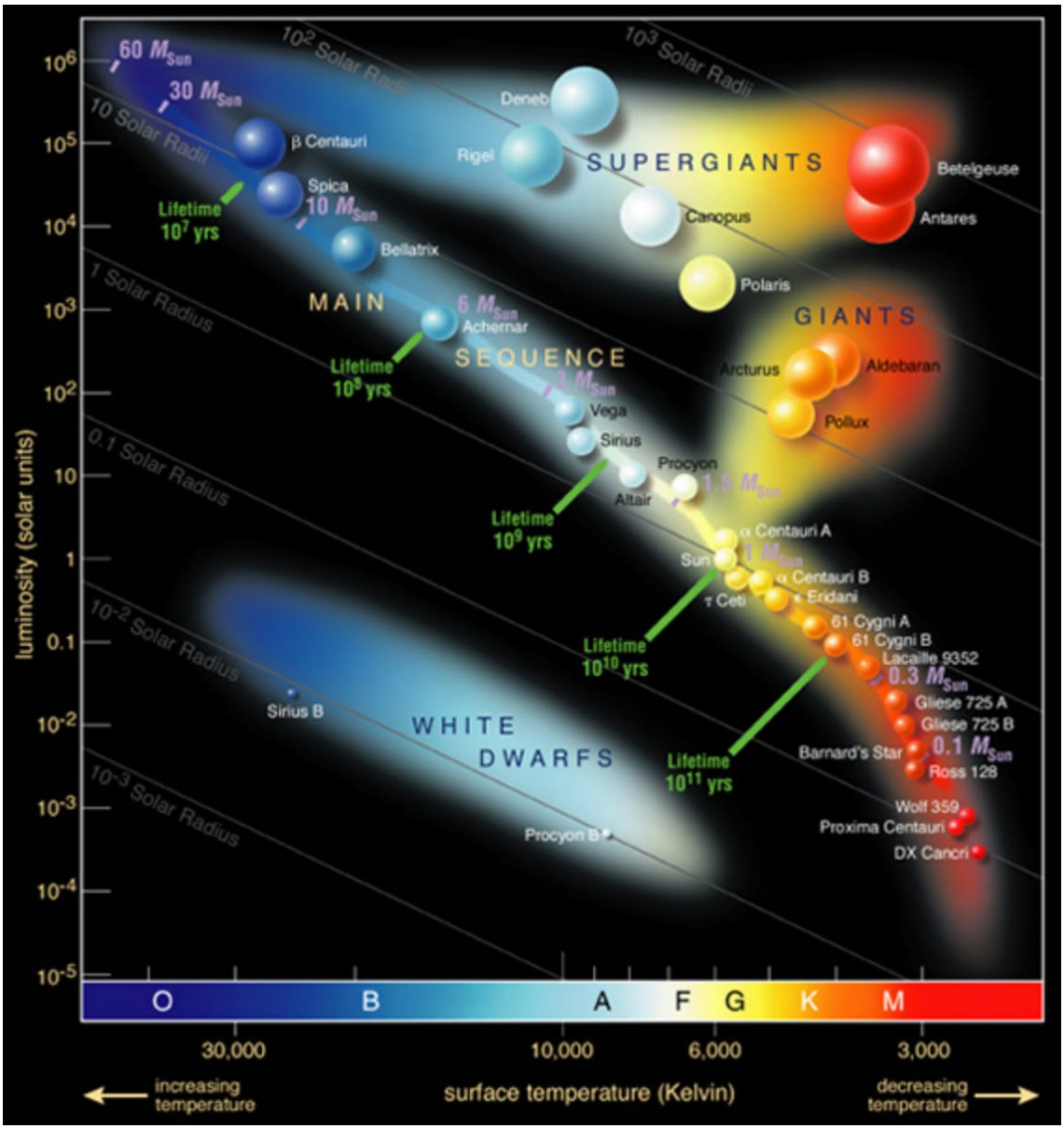

Figure 1.1: The Hertzsprung-Russell (HR) diagram.

is no longer maintained, and it collapses and becomes a supernova.

$$\frac{dP}{dr} = -\frac{GM_r\rho_r}{r^2} \tag{1.3}$$

In Eqn. 1.3 P is the pressure, M_r is the mass of the interior within the radius r, and ρ_r is the density of the star. The equation for pressure suggests that the increase in pressure due to the increase in nuclear fusion at its core expands the radius of the star. This means that the star must maintain the pressure proportional to its mass and density to be in hydro-static equilibrium.

Main sequence stars with initial mass above roughly 8 $M_\odot$ end up their lives as neutron stars (NSs), black holes (BHs), or massless remnants. In the numerical simulation presented in this work, we have used the mass range of 8 to 100$M_\odot$, which may allow the formation of white dwarfs (WDs) in some mass transfer scenarios , but the primary focus of of our study is NSs and BHs.

1.4 Binary Interaction

Binary stars are influenced by each other and their evolution depends on their interaction with each other because of their combined gravitational potential. In the binary system the hydro-static equilibrium is challenged due to the mass transfer. The mass accretion process can thus accelerate the stellar evolution. The combined potential creates a Roche Lobe around a star because of the equipotential geometry of the gravitationally bound object as shown in Figure 1.3.

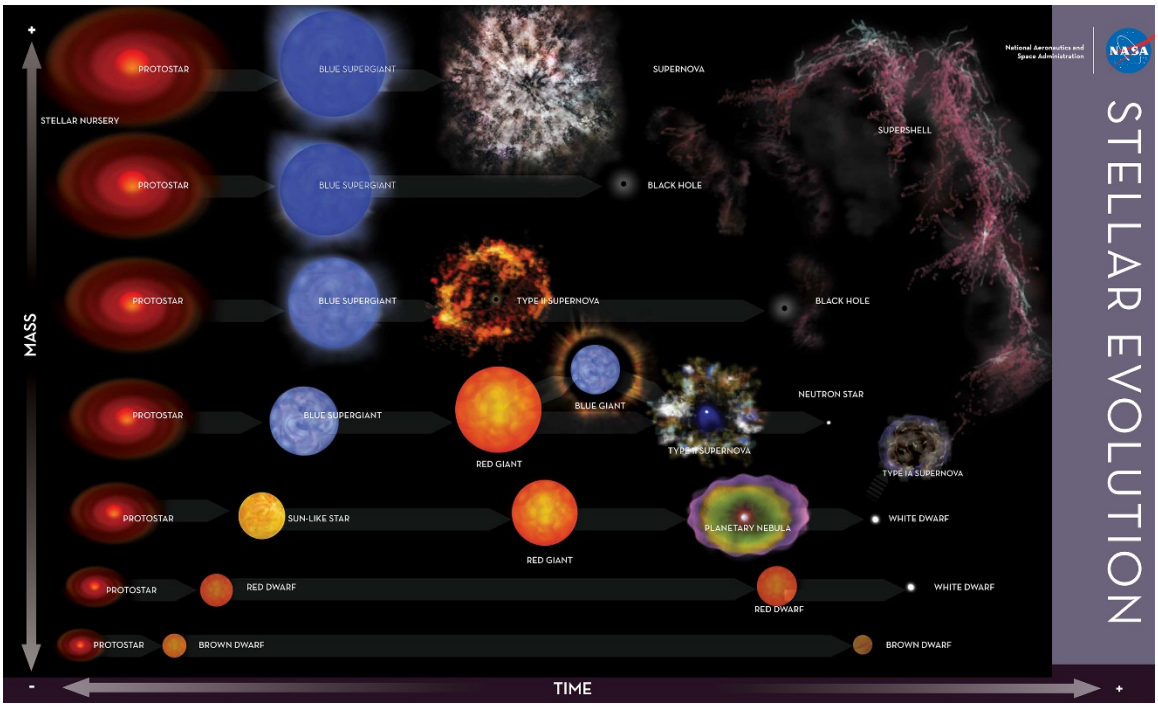

Figure 1.2: Stellar Evolution illustrated in terms of Mass v. Time; Source: NASA

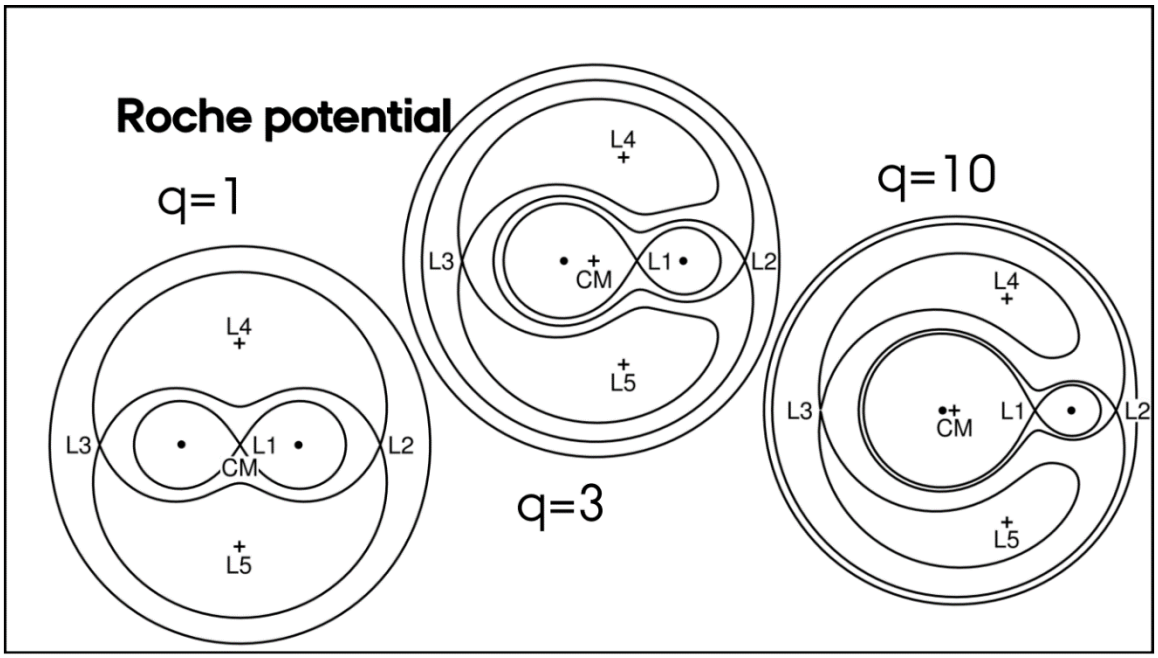

Figure 1.3: Roche Lobe Potential; Source: O. Pols, Lecture notes, Utrecht University

The Roche Lobe radius of the secondary star can be found using the Eggleton equation:

$$r_L = \frac{0.49q^{\frac{2}{3}}}{0.69q^{\frac{2}{3}}ln\left(q+q^{\frac{1}{3}}\right)}a \tag{1.4}$$

where $q = m_1/m_2$, m_1 is the mass of donor, m_2 is the mass of the accretor, and $a = a_1 + a_2$, with a_1 is the semi-major axis of m_1,, and a_2 is the semi-major axis of m_2. When the m_1 fills out its Roche Lobe surface, steady mass transfer onto the m_2 star occurs (Casares et al., 2009). A classical example is the binary star β Lyrae (Figure 1.4).

Stable Mass Transfer: Stable mass transfer occurs when the angular momentum of the circular binary is conserved. Angular momentum of the binary system is given by:

$$L = m_1 m_2 \sqrt{\frac{G\left(a, +a_2\right)}{m_1 + m_2}} \tag{1.5}$$

During the mass transfer the donor star m_1 loses its mass to m_2. If the donor star is more massive compared to its companion, the orbit of the system shrinks and if the less massive star is the donor, the orbit expands preserving the angular momentum of the system. During the stable mass transfer, it is possible that the less massive star accretes mass from its more massive donor and becomes more massive before the supernova explosion (SNe) of the primary. The more massive star is usually the one that fills the Roche Lobe and becomes the donor (Benacquista, 2013).

Unstable Mass Transfer:

Unstable transfer occurs when the mass transfer does not preserve the angular momentum of the binary system. One of the ways for the mass transfer to be unstable is when the

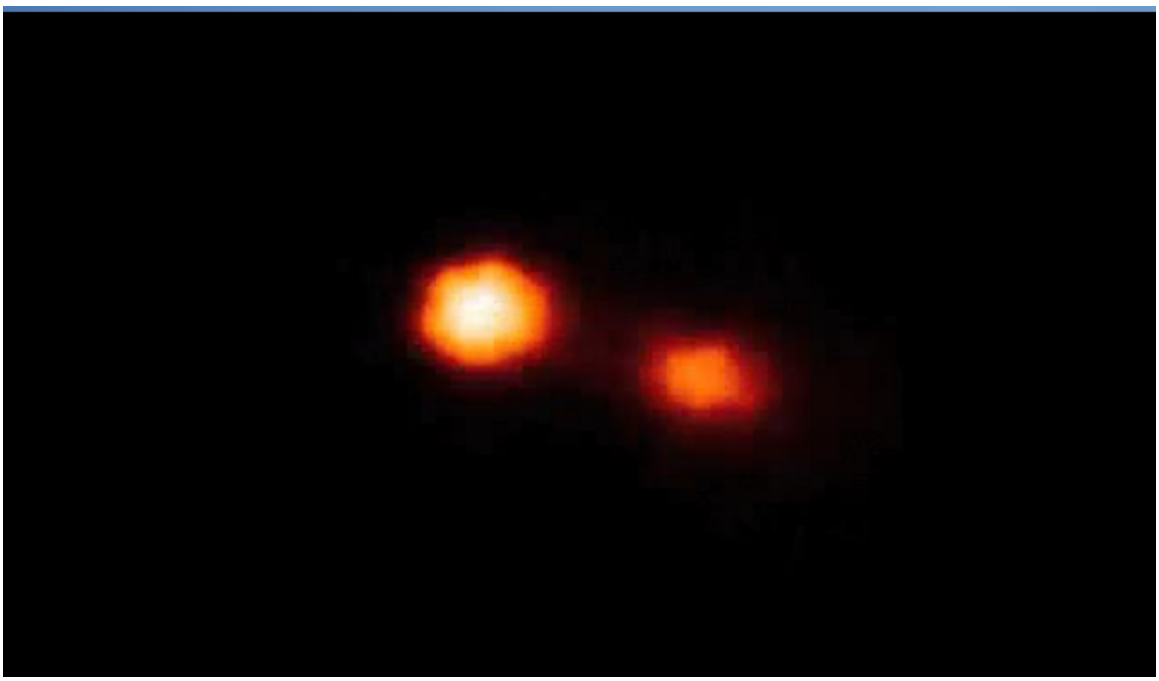

Figure 1.4: First Resolved Images of the Eclipsing and Interacting Binary β Lyrae. Source: (Zhao et al., 2008)

donor star expands beyond the Roche Lobe limit and encompass the companion in the common envelope. Another way of unstable mass transfer occurs when the donor star transfers its mass faster than a companion can accrete.

1.5 Supernova

When a massive star exhausts its nuclear fuel, it can no longer exert pressure to withstand its own gravity and the star collapses into its own core and then the SNe occurs and a compact object is left behind, a NS or a BH. The focus of this work is what happens with such stellar remnants, and we will not discuss the evolution of low mass stars.

In binary star systems, stellar evolution is accelerated due to the mass transfer. When a star accretes mass from its companion it can no longer sustain its increased mass and the star becomes supernova (SN) faster. There are two main classes of SNe, core-collapsed and exploding WD (Ia).

- Core-collapsed Supernova: Evolution of the binary stars, especially the close binaries, accelerate due to the Roche Lobe overflow. It has been calculated that 20 to 30% of supernovae in the binary are type II supernovae (Joss, 1996). There are multiple ways that the binary stars become progenitors of the type II supernovae. One of the scenarios is that the more massive star fills up its Roche Lobe and looses its mass to less massive companion and the merger could occur. If the donor star were in main sequence before the mass transfer, the merger (merged star) could be new rejuvenate main sequence star. One of the likely appearances of this star will be that of red supergiant and the progenitor of typical type II supernovae. Merger could also be blue supergiant and the progenitor of type II supernovae. Another interesting situation occurs when a star in the binary accretes mass from its donor and the accreting star completes its main sequence phase and end its life either as a type II or type Ib/Ic supernovae (Joss, 1996).
- Type Ia: Type one is the name given to a supernova in a binary with one white dwarf and a companion. When the white dwarf accretes mass from it's companion it meets the Chandrashekar limit of 1.44 $M_\odot$ (solar masses) and becomes SN. White dwarf are usually remnants of low mass stars, and, therefore, in this work we only focus on Type 2 SNe.

During SNe massive amount of energy is released

$$\frac{3GM}{5R^2} \simeq 3 \times 10^{53}\, erg \tag{1.6}$$

which is roughly 10% of its total mass energy (Lattimer and Prakash, 2004).

Asymmetric Supernova Kick

Observational evidence suggests that the SNe are more likely to be asymmetric. Asymmetry in the SNe creates a dipole moment in the aftermath of a supernova; a compact object that forms after the explosion runs away in the opposite direction of ejecta (see Figure 1.5) Holland-Ashford et al. 2017. An asymmetric SN is independent of the systems, binary and non-binary.

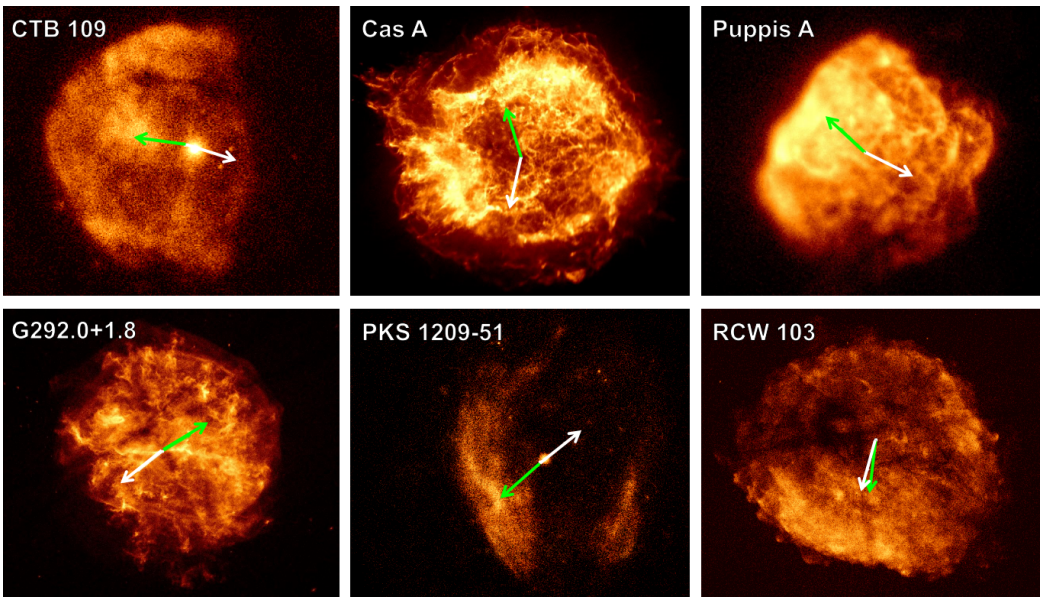

Figure 1.5: Asymmetric Supernova explosion; Direction of NS motion(white arrow). Source: (Holland-Ashford et al., 2017)

The asymmetric SN-kick model used in our numerical simulations is based on Tauris and Takens (1998) deduction of the statistical study of pulsars by Gunn and Osticker 1970; the magnitude of the "kick" follows The Maxwellian Distribution (Equation 1.7) (Tauris and Takens, 1998).

$$f(V_K)dV_K \;=\; 4\pi {V_K}^2 (2\pi {\sigma_{V_K}}^2)^{-3/2} e^{(-{V_K}^2/2{\sigma_{V_K}}^2)} dV_K \tag{1.7}$$

where mean of V_K is roughly 300 km/s and represents the magnitude of the mean "kick".

1.6 Compact Objects

White Dwarves

There is an upper limit of mass that suggests that our sun is one day going to explode and become a WD, and the limit is known as Chandrasekhar Limit. If a star's core (stellar remnant) exceeds $1.4\,\mathrm{M}_{\odot}$, it will not be a WD; it either becomes a NS or a BH. The equation that suggests this is a robust consequence of classical physics and quantum physics.

$$M_C = \frac{15}{64}\,(5\pi)^{1/2}\,\frac{(\hbar CG)^{\frac{1}{2}}}{m_p^2} \approx 1.4\,M_{\odot} \tag{1.8}$$

After the star exceeds this mass limit, the degeneracy pressure of electrons can no longer sustain the gravity and the star collapses under its own gravity especially if it is a sun like star in the binary system and has been accreting mass from its donor.

Neutron Stars

NSs are core collapsed stars typically greater than $1.4\,\mathrm{M}_{\odot}$ and radius of roughly 12 km; they are some of the densest matters in the Universe. NSs are almost entirely composed of neutrons with a small amount of proton and electrons. Depending on the viewing angle of the observer, some NSs are classified as pulsars, from which highly periodic pulses are detected in. the radio and X-rays. When a star of greater than eight solar mass becomes a type II SN, it is likely to be a NS. The core collapse stops when the neutron degeneracy pressure can support the compact object.

Black Holes

Black holes forms when a star collapses into a singularity, and not even light can escape from it. Schwarzschild's description of the spherically symmetric black hole was theorized

initially from the solution to the Einstein Field Equations. The Schwarzschild's radius is

$$R = \frac{2GM}{c^2} \tag{1.9}$$

where R is the radius, M is mass, G is gravitational constant, and c is the speed of light.

1.7 Stellar Evolution Code

We use the binary population code `binary_c` to generate a population of binary stars and follow the evolution of their stellar properties over time (Izzard, 2004; Izzard et al., 2006). The code is based on the rapid binary evolution code BSE (Hurley, 2000), which uses stellar models by Pols et al. (1998).

There is substantial observational evidence that most massive stars formed in binaries (Kouwenhoven et al., 2009). Here we assume that all massive stars are formed in binaries, and, therefore, we can use `binary_c` to simulate the entire population of massive stars in our study. While the binarity of massive stars is well established, very little is known about the population of binary parameters (masses, orbital period, eccentricity). We consider two main families of models as described below.

Model 1(M1):

We use binary parameters as described by Kroupa et al. (1993). We generate binaries with masses in the range of 8 to 100 $M_\odot$ randomly drawn from a Salpeter initial mass function (IMF), which is a power law with a slope of -2.35. The mass range is selected so that only massive stars are included in our study. This allowed us to study the distribution of NSs and BHs.

The eccentricity distribution follows

$$e(X) = (X)^{1/2} \tag{1.10}$$

where X is uniformly distributed from 0 to 1. And the generating function for semi major axis(a) is given by

$$a(X) = a_{min}(10)^{X(log_{10})(a_{max}/a_{min})} \tag{1.11}$$

where $a_{max} = 1690$ AU, and $a_{min} = 1.69$ AU.

Model 2(M2): Model 2 is based on the parameters by Sana et. al., 2012. The parameters are extracted from the observed data of sample of 71 O-Type stars. The observation campaign finds that the evolution of binary systems are drastically influenced if the stars are within 1500 days period. These are spectroscopic binaries, observed over a period of 10 years. The study suggest that the initial orbital period distribution follows a power log distribution.

$$f_p(\log p) = (logp)^{\pi} \tag{1.12}$$

where $\log p(days) = [0.15, 0.35]$, and $\pi = -0.55 \pm 0.2$.

The distribution of the mass ratio is given as

$$f_q(q) = q^k \tag{1.13}$$

where q is a mass ratio of $M_</M_>$, $q = [0.1, 1]$, and $k = -0.1 \pm 0.6$q.

2. COMPACT OBJECTS IN BINARY SYSTEMS

Once massive stars run out of fuel, there are two main endpoints of stellar evolution: NS or BH. When a star in a binary system explodes, turns into a compact object and does not receive a kick over a certain threshold (kinetic energy > gravitational potential energy), it remains in the binary system. In roughly 2/3 of binaries, however, the system is disrupted by the asymmetric SN kick.

In a recent study, it is observed that MAXIJ1535-571 is a black hole with a companion in a supernova remnant, and it is highly likely that the progenitor was a close binary system (Maxted et al., 2020). In 2017 LIGO and VIRGO announced that they had detected the gravitational waves from the collision of two black holes of 12 and 7 solar mass. Another announcement was made in the same year of the detection of gravitational waves from colliding neutron stars followed by simultaneous measurement of γ-ray burst. These are a few examples of interesting binary scenarios. In this Chapter we look at the binaries that contain at least one compact object. In the numerical simulation, we use a mass range from 8 to 100 $M_{\odot}$, which allowed us to focus on stars capable of producing NSs and BHs. Some of the results from our simulations for Model 1 and 2 are shown in Table 2.1. We explore four different metallicities for each model.

2.1 Double-Degenerate Binary Systems

We know very little about the parameters of double-degenerate binaries due to the very limited observational data. Such systems are non-accreting and thus have no electromagnetic signatures. Only pulsars can be detected but only if viewed from a preferential angle with respect to their spin axes. With the help of facilities such as LIGO and VIRGO, we can now detect gravitational waves from mergers, however, we can only put constraints on the masses of the merging objects rather than the binary parameters

Table 2.1: Number of different binary states after the supernova

Metallicity	NS-Companion Binary	NS-NS Binary	BH-BH Binary	BH-Companion Binary	NS-BH Binary
Model 1					
0.0001	3684 ± 60	74 ± 9	11 ± 3.3	1527 ± 39	128 ± 11
0.001	4218 ± 65	644 ± 25	14 ± 3.7	1201 ± 34.6	81 ± 9
0.01	4100 ± 64	471 ± 21.7	2 ± 1.4	914 ± 30.2	92 ± 9.6
0.02	4312 ± 65.7	372 ± 19.3	2 ± 1.4	1056 ± 32.5	156 ± 12.5
Model 2					
0.0001	7347 ± 85.7	164 ± 12.8	74 ± 8.6	2303 ± 48	169 ± 13
0.001	6227 ± 79	598 ± 24.4	44 ± 6.6	1736 ± 41.6	139 ± 11.8
0.01	6063 ± 81.2	430 ± 20.7	11 ± 3.3	1304 ± 36.1	384 ± 19.6
0.02	6016 ± 77.6	334 ± 18.3	12 ± 3.5	1350 ± 36.7	486 ± 22

prior to the merger event. As such, numerical simulations can allow us to look into the formation and evolution of such systems.

Double Neutron Stars

When a star in a binary system becomes a SN and does not escape the system, we have a NS and a companion binary. When the companion also becomes a SN (at a later time) and does not escape the system, we have double NS binary. We know that the double NS binaries exist from the detection of gravitational waves from double neutron star mergers and the radio detection of binary pulsars. Our numerical simulation suggests that double NS binaries are one of the least likely outcomes. Model 1 generates 0.148%, 1.29%, 1%, and 0.744% NSs binaries out of 50, 000 binary systems for metallicities 0.0001, 0.001, 0.01, and 0.02 respectively. For Model 2, only 0.33 %, 1.2 %, 0.86 %, and 0.67 % turn into double NSs binaries for metallicities 0.0001, 0.001, 0.01, and 0.02 respectively.

In comparison with Model 1, Model 2 generates fewer double NS states on average. One qualitative prediction of the simulation is that double NS binaries are likely to be close binaries if their progenitors are metal-poor stars (metallicity 0.0001).

Double Black Holes

Double BH binaries are the rarest among the binariy outcomes, and they are the hardest, if not impossible, to observe. Occasionally we detect gravitational waves when binary BHs merge. Our numerical simulations also show that a double BH binary is seen least frequently. Out of 50,000 binary systems, only 0.02% for the metallicities 0.0001 and 0.001 turns into black hole binaries. It is virtually nonexistent in the case of metallicity 0.01 and 0.02 for Model 1.

The double BH binaries in the Model 2 follow the same trends as Model 1. Out of 50,000 binary systems, numerical simulation generates 0.148 %, 0.088 %, 0.022%, and 0.022 % for metallicities 0.0001, 0.001, 0.01, and 0.02, respectively. We do see in increase of BH-BH formation with decrease of metallicity. While Model 1 shows similar trend, the numbers are too low to confidently make such statement.

Neutron star and a black hole binary

NS-BH binaries for Model 1 are 0.25%, 0.16%, 0.18%, and 0.31% for the metallicities 0.0001, 0.001, 0.01, and 0.02 respectively. According to the model, the formation of the NS-BH binary is slightly more likely for the metal-rich star and first-generation stars with low metallicity compared to intermediate stars in terms of metallicity.

Model 2 shows the formation of BH-NS state to be slightly more likely compared to BH-BH state and slightly more likely than NS-NS state. Out of 50,000 binary systems only 0.34%, 0.28%, 0.77%, and 0.97% become the NS-BH binary for metallicities 0.0001, 0.001, 0.01, and 0.02 respectively.

2.2 Binaries with a Compact Object and Non-Degenerate Star

A large number of SNRs have been detected where the a NS is located in the vicinity of the remnant. However, there are very few confirmed cases where a binary is still present in the SNR after the explosion. Due to observational difficulties, the exact number of SN

that still host a binary remains unclear. Our study can shed light into this issue.

Another reason binary systems with one compact object are of great interest is because they could potentially turn into X-ray binaries (XRBs). There are two general types of XRBs: low- and high-mass X-ray binaries (LMXBs and HMXBs, respectively). The name of these two types comes from the type of companian stars. For example, HMXBs are binaries where one member of the system is a compact object, either a BH or NS, and the other is a young, massive star. X-ray emission is produced as material is accreted from the young "donor" star onto the compact object. In LMXBs, the companian star is a low-mass star.

Neutron Star and a Companion Binaries

NS and a companion binary is the most likely state after the supernova explosion in the binary system. Out of 50,000 binaries numerical simulation for model 1 generates 7.368%, 8.436%, 8.2%, and 8.62% NS-Companion binary for metallicities 0.0001, 0.001, 0.01, and 0.01 respectively. Numerical simulation for Model 2 suggests that out of 50,000 binary systems, 14.7 %, 12.45%, 12.13%, and 12.03 % for the metallicities 0.0001, 0.001, 0.01, and 0.02 respectively remain as a neutron star and a companion binary in the aftermath of SNe (Table 1). Model 2, compared with Model 1, generates more of NS-Companion binaries. This is also true for other types of binaries. This effect is a result of the parameters of Model 2, which produce much tighter binaries compared to Model 1. We also notice that the number NS-Companion binaries is higher for metal-poor systems. In contrast, Model 1 has roughly the same fraction of the NS-Companion binary except for the metallicity of 0.0001, which is not common throughout the simulation.

Black Hole and a Companion Binaries

Stellar evolution code suggests the formation of a BH and a normal star companion binary is frequent. Numerical simulation shows that out of 50,000 binary systems, 3%, 2.4%, 1.8%, and 2.1% become BH-Companion binary for metallicities 0.0001, 0.001, 0.01, and

0.02 respectively. For Model 2, the numbers are relatively higher: 4.6%, 3.5%, 2.61%, and 2.7% for metallicities 0.0001, 0.001, 0.01, and 0.02 respectively.

BH- and NS-companian stars are short lived binaries (usually lasting tens of Myrs at the most). As such, they are associated with regions of recent star formation. This is consistent with observation with HMXBs, which are primarily found in star-burst galaxies (Fabbiano, 2006; Prestwich et al., 2003; Rangelov et al., 2011, 2012).

3. HIGH VELOCITY RUNAWAY STARS

In the recent study of a supernova remnant, a runaway star (HD37424) was identified with a peculiar velocity of 74 ± 8 km/s. When it was traced back to its origin, it was found to be at the location of the central compact object, a pulsar (PSR JO538+2817). The central compact object and the runaway star were binary stars before the supernova explosion (Dincel et al., 2015). This was a lucky finding, but it is improbable that we get to trace back the origin of the runaway stars, especially if there is no supernova remnant nearby. There are also some speculative suggestions that PSR J0826+2637 and runaway supergiant G0 star HIP13962 share a common origin (Tetzlaff et al., 2014). In another example, the runaway O-Star (VFTS102) and young pulsar PSRJ0537-6910 originate from a binary system in The Large Magellanic Cloud (Dufton et al., 2011) demands further study into the origin of runaway stars. To study the origin and the velocity of the runaway stars, we have come up with the sample of 50,000 binary stars that give birth to significant fraction (see Table 3.1, 3.2, and 3.3) of runaway NSs, BHs and normal stars (companions).

A few studies of pulsars with high velocities; Hobbs et al. (2005) show that the 3-D birth velocity follows a Maxwell-Boltzmann (MB) distribution with a mean velocity of 400 ± 40 km/s, and 1D RMS $\sigma = 265$ km/s. Another study by Lyne and Lorimer (1994) shows that pulsars at birth follow the MB distribution with a mean speed of 450 ± 90 km/s. However, the sample size in the study by Hobbs et al. (2005). contains 73 pulsars with characteristic age of <3Myr, and the sample size of the study by Lyne and Lorimer has only 29 pulsars.

3.1 High Velocity Neutron Stars

One of the complete data we have on high-velocity pulsars is from the study of 73 pulsars with proper motion measurement, and a wide variety of pulsars including recycled objects

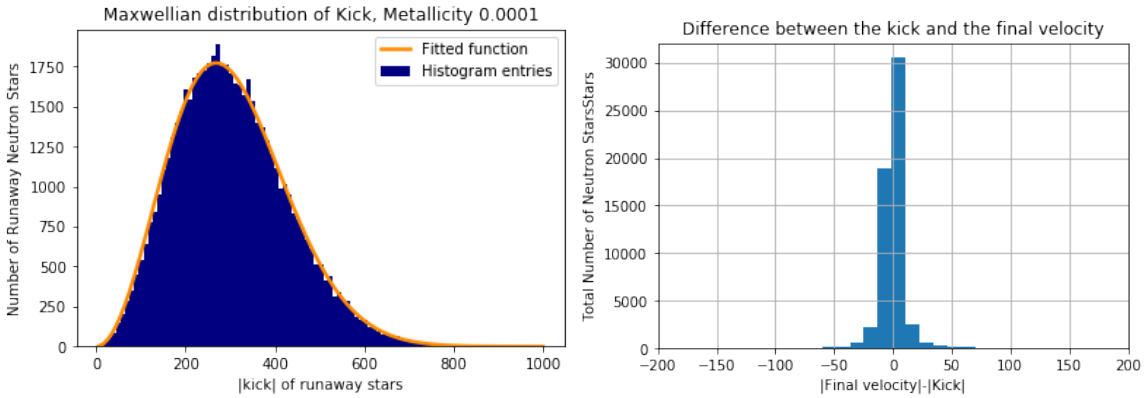

Figure 3.1: Maxwellian distribution of the magnitude of kick imparted on runaway stars during the SNe (top), and histogram representation of the difference between the final velocity and the kick (bottom).

and those associated with globular clusters or supernova remnants (Hobbs et al., 2005). The authors used a novel deconvolution technique on the sample of 73 pulsars with characteristic ages <3 Myr to obtain a mean 3D pulsar birth velocity of 400 ± 40 km/s. Hobbs et al. (2005) conclude that there is no evidence for a bimodal velocity distribution.

Velocity Components with Respect to the Binary Plane

All velocity components were calculated with respect to the plane of the binary prior the SNe. The primary star (first star to become a SN) is at the origin of the Cartesian coordinate system. The positive x-axis points towards the direction of the initial velocity of the primary star along the orbit before the SN. The positive y-axis points toward the center of mass and also the companion star. Positive z-axis is perpendicular to the x-y plane indicates the direction of the orbital angular momentum, using the right-hand rule. The distribution of all three components are symmetrical, with V_Y showing double peaks (Figure 3.3, and 3.4). The component V_Z concentration in the high-velocity is more limited in range compared to the other two axes.

Using the three velocity components, we can calculate the trajectory of the runaway NS in its original frame of reference. Velocity components are of much higher magnitude on the x and y axes compared to the z axis, which means that NSs are more likely to run away

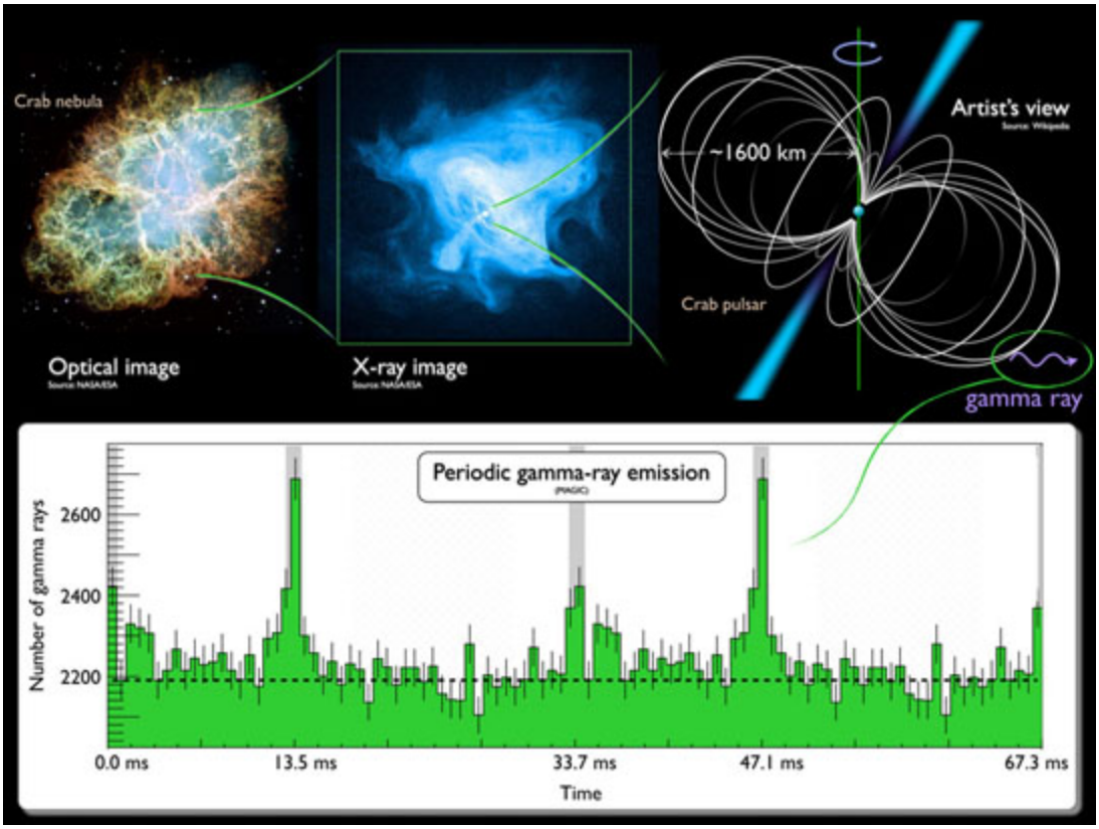

Figure 3.2: Crab Nebula via optical telescope (left), x-ray telescope (middle), and the artist illustration of magnetic field (right). Histogram representation on the bottom shows the gamma rays interval of 0.0337 seconds. Credit: NASA, ESA, J. Hester, A. Loll, CXC, SAO, F. Seward et al., MAGIC Collaboration

parallel to their progenitors' original plane of rotation. Distributions are virtually the same regardless of metalicity or model, which, again, can be explained by the SN kick dominating the velocity.

The Maxwellian distribution of the NS runaway velocity (Figure 3.5 and 3.6), acquired during the SNe and binary disruption, has a mean of $\sim$300 km/s for both Models 1 and 2. These numbers are indistinguishable from those of the SN kick itself. The difference between the final velocity and the SN kick (Figure 3.1, bottom) is within the margin of error ($\pm$10 km/s). The histogram shows that while the SN kick and NS final velocities are statistically the same for the entire populations, there a small numbers of sources, for which being in a binary can result in significant difference from being born in isolation.

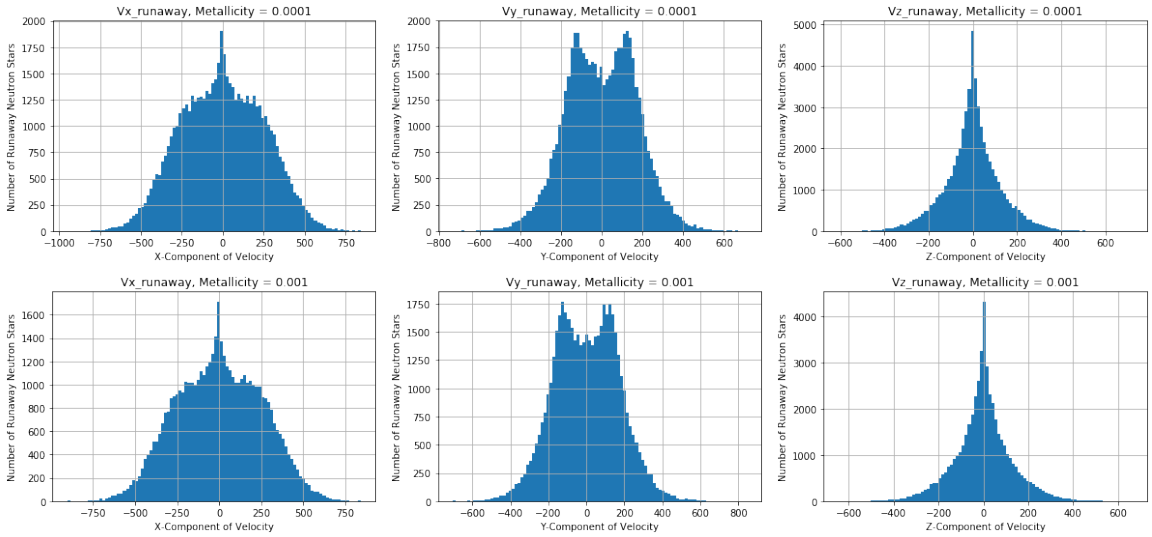

Figure 3.3: X, Y, and Z Components of the final velocity of neutron stars from left to right for metallicities 0.0001 and 0.001 of Model 1

The mean of the distribution suggests the kick imparted during the SN dominates the magnitude of final velocity. As such, we cannot make any distinction between runaway NS originating from binaries or from isolated stars.

Figures 3.3 and 3.4 show the runaway NS velocity components with the metallicities of 0.0001, and 0.001 for Model 1 and Model 2, respectively. Velocity components in the Original frame of reference suggest that the V_F is highly likely to be perpendicular to the z axis of the original binary orbit, given the angle between V_F and V_Z.

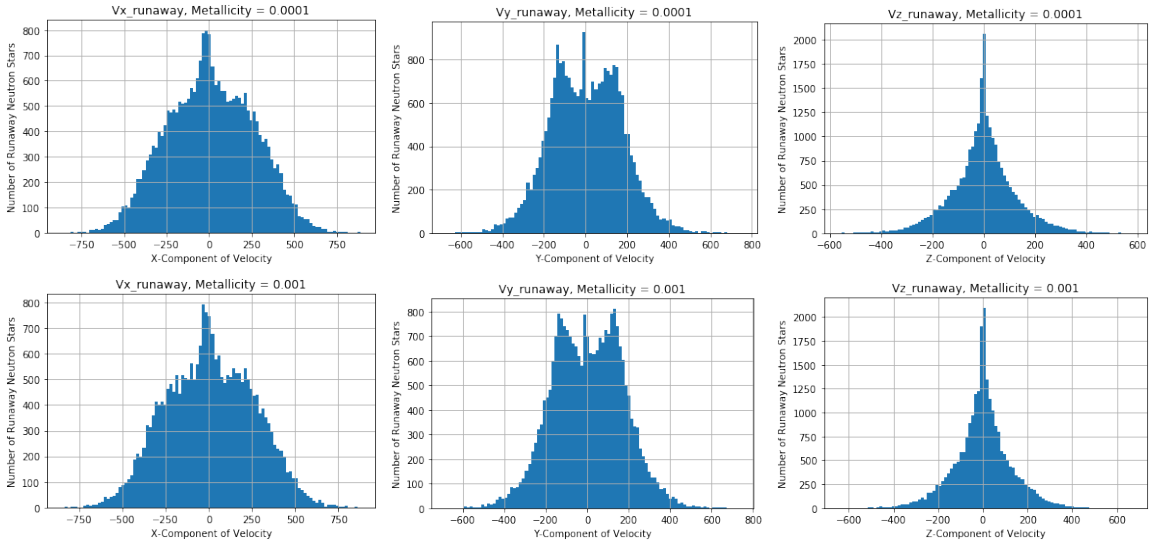

Figure 3.4: X, Y, and Z Components of the final velocity of neutron stars from left to right for metallicities 0.0001 and 0.001 of Model 2

Final velocity in the original frame

The final velocities of the runaway NSs in the original frame obey the Maxwell-Boltzmann (MB) distribution. The MB distribution of the metallicity of 0.0001, 0.001, 0.01, and 0.02 has an average velocity of approximately 300 km/s; the mode of the distributions has roughly 266 km/s. Mean, mode, and sigma roughly the same for all metallicities. Around 7.6% of the total runaway NS population of all metallicities exceeds the velocity of 500 km/s, and roughly 2% exceeds 750 km/s. These will be considered hyper-velocity NSs. It is interesting to note that the number of hyper-velocity NSs increases for metal-poor stars in Model 1, while we do not see the same trend for Model 2 (number remain roughly the same) within the margins of error. We do see a similar correlation between Model 1 and 2 for the total number of runaway NSs. Note that the of initial binary separations in Model 1 is much wider compared to Model 2, and, therefore, binaries in Model 1 are much easier to be disrupted and produce more runaway NSs. For Model 2, roughly 5.6% of the runaways exceed 500 km/s, and about 0.124% exceed 750 km/s. Population difference in Model 2 does not differ for metallicities like Model 1.

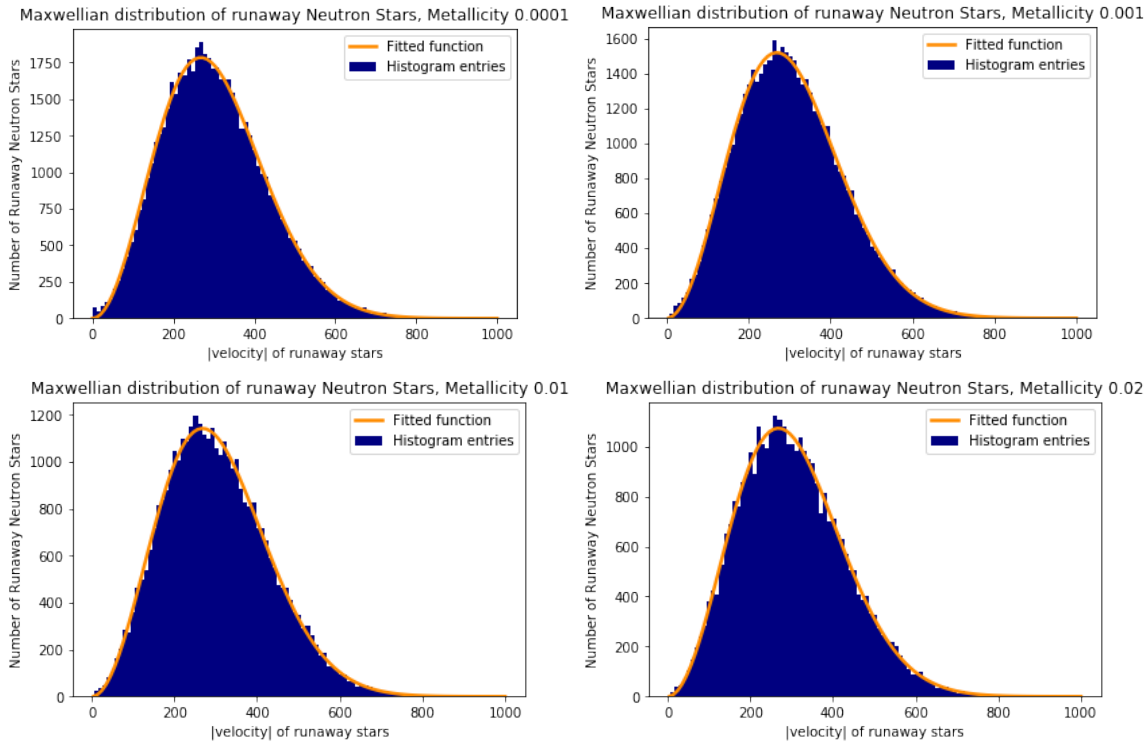

Figure 3.5: Maxwellian distribution of the final velocity of the runaway neutron stars in the original frame for Model 1.

Table 3.1: Numerical results from the Velocity Distribution in Maxwellian of the Runaway-NS in an original frame.

Metallicity	Runaway-NS	Mean	Mode	Sigma	>500 km/s	>750 km/s
		km/s	km/s	km/s		
Model 1						
0.0001	56940 ± 238	302	269	128	4163 ± 64	88 ± 9
0.001	49104 ± 221	303	269	128	3631 ± 60	84 ± 9
0.01	36867 ± 192	303	269	128	2732 ± 52	46 ± 6
0.02	34707 ± 186	300	266	127	2559 ± 50	47 ± 6
Model 2						
0.0001	24968 ± 158	303	269	128	1971 ± 44	47 ± 6
0.001	24588 ± 156	304	269	128	1877 ± 43	54 ± 7
0.01	25998 ± 161	302	268	127	1967 ± 44	39 ± 6
0.02	26330 ± 162	302	268	127	2020 ± 45	42 ± 6

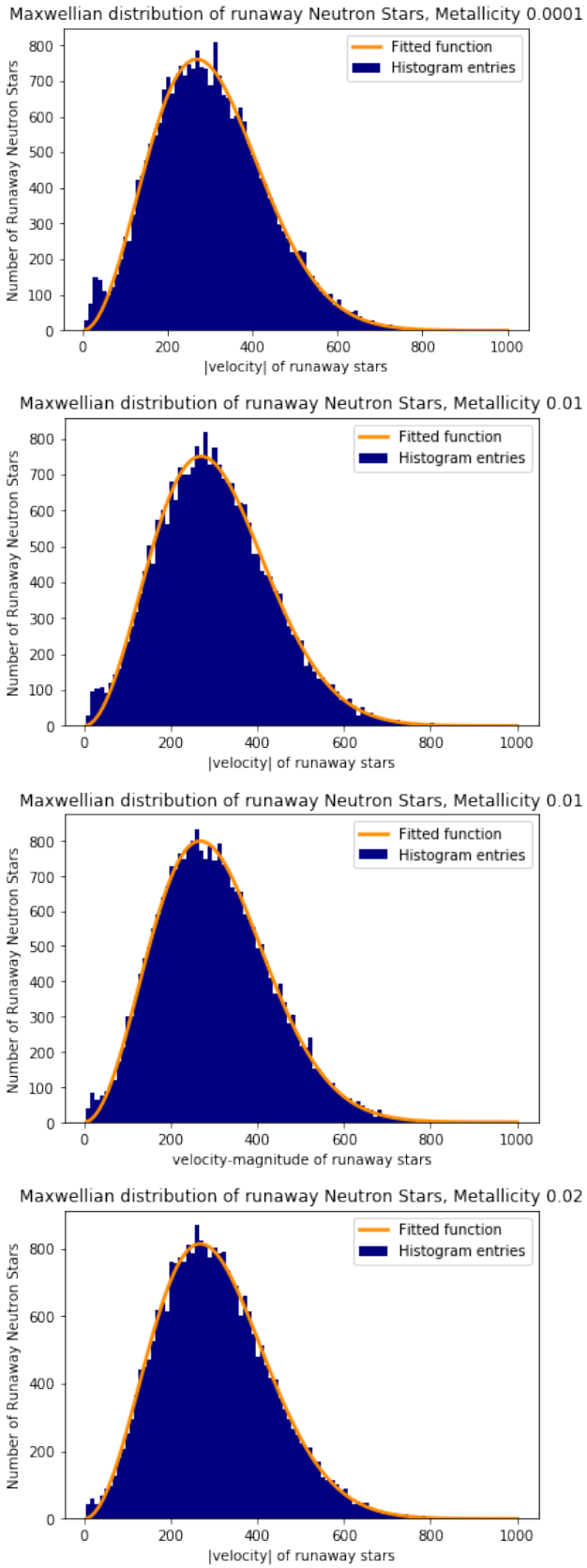

Figure 3.6: Maxwellian distribution of the final velocity of the runaway neutron stars in the original frame for Model 2.

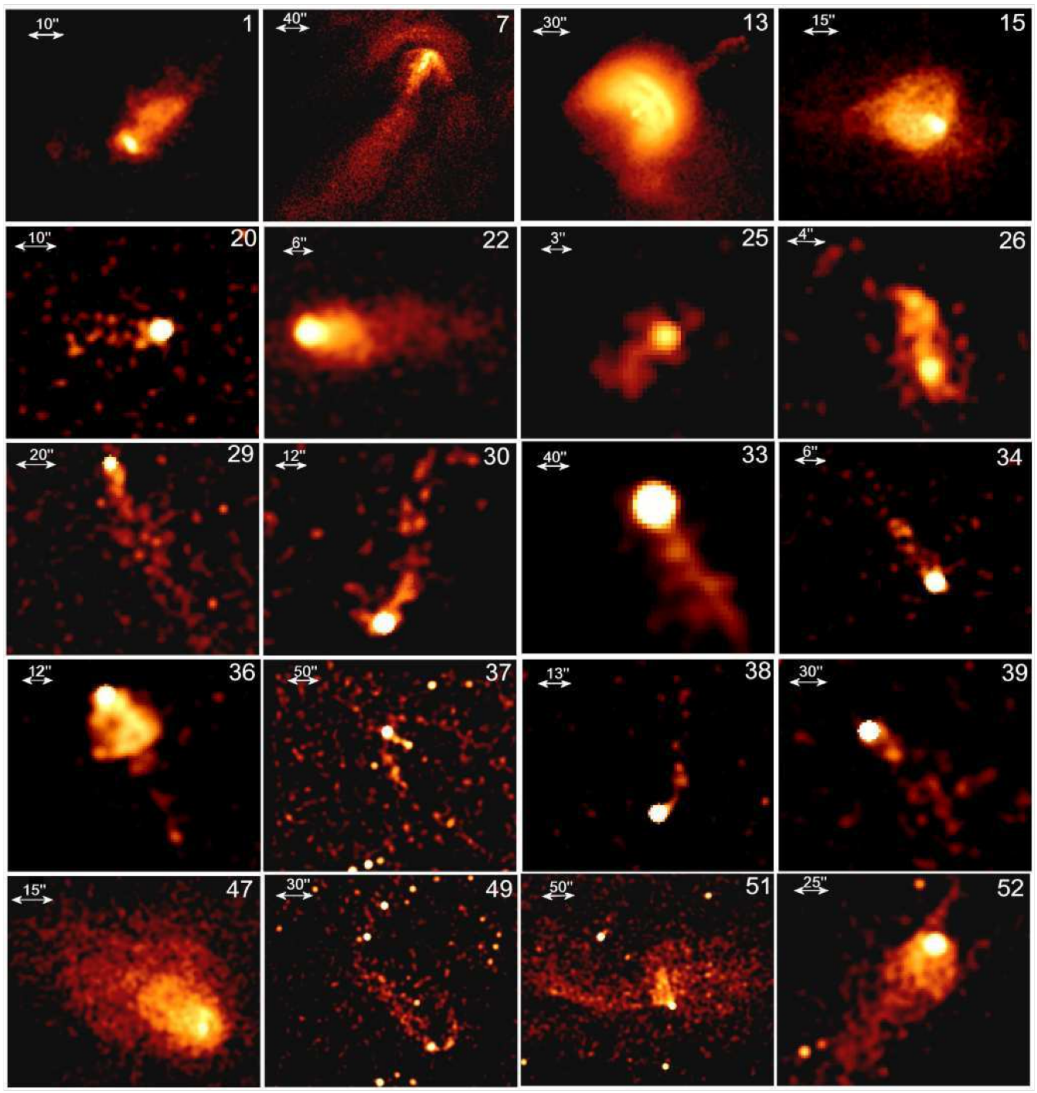

Figure 3.7: X-ray images of PWNe whose shapes are affected by the pulsar motion. Adopted from (Kargaltsev and Pavlov, 2008).

3.2 Preferential Spin-Axis

Pulsar winds shocked in the ambient medium produce nebulae detectable from the radio observations through γ-rays. The shape of a pulsar wind nebula (PWN) depend on a number of properties: angular distribution, magnetization, pulsar velocity and the properties of the ambient medium (Kargaltsev and Pavlov, 2008). In recent decades, the Chandra X-ray Observatory, with its unprecedented angular resolution and sensitivity, has allowed us also study many PWNe, and their structure and dynamics.

Figure 3.7 shows that the PWNe morphologies can vary drastically. Some pulsars have "Mushroom" PWN (e.g., #36, Figure 3.7), which consists of a broad, bright "cap" and a narrow, faint "stem". The Geminga PWN (#37) shows a shell-like structure with a bow head, and a short, narrow tail (possible jet) along the symmetry axis of the shell. Other types of PWNe have bow shaped X-ray tails, often aligned with an Hα bowshock, in the direction of the pulsar's proper motion. It is clear that the morphology of PWNe may significantly depend on the orientation of the spin axis with respect to the direction of pulsar's motion. Nevertheless, the origin of the diverse, often very complex, PWN morphologies still remain elusive. Here we use numerical simulation to shed some light on this problem.

Given that the NS spin axis orientation with respect to the direction of pulsar's motion (which we call here preferential spin-axis angle) can play a crucial role, we determine this angle from our simulations. While we know the exact components of the runaway velocities, this angle is not a direct product from the code. Thus, we assume that the spin axes of both stars in the binary is perpendicular to the orbital plane. While this may not be strictly true for individual cases, for a population study such as ours it is a good approximation. Using this assumption, we calculate the angle between the NS final velocity and the z-axis of the binary orbit to get then preferential spin-axis angle.

Figure 3.8 shows the distribution of the preferential spin-axis angle. Our results show that the peak of the distribution is at $90°$. This suggests that most runaway NS have their spin-axis (and potential jets shooting out) perpendicular to the direction of motion. This may explain why some pulsars have bow like streaming tails behind these pulsars.

Velocity Distribution of Neutron Stars in the Projected Frame of Earth

For many observed runaway stars (regular or NS), we cannot calculate their true 3D velocity through space. In most cases, we only have their tangential velocities from proper motion measurements. To compare our results to these data, we have calculate projected

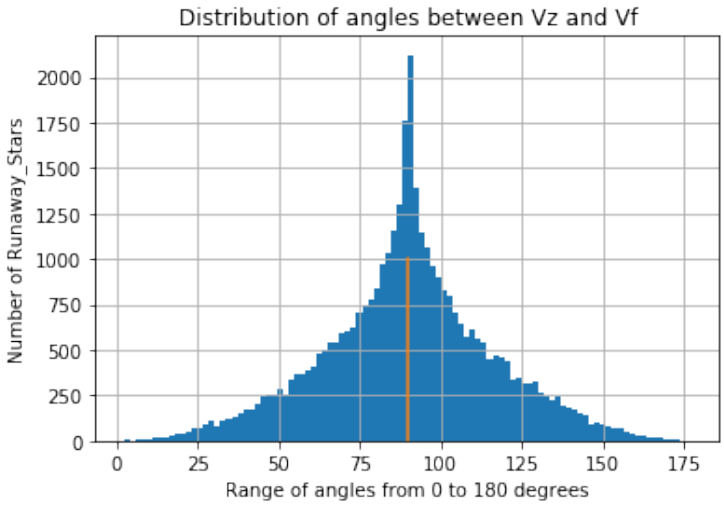

Figure 3.8: Preferential spin-axis.

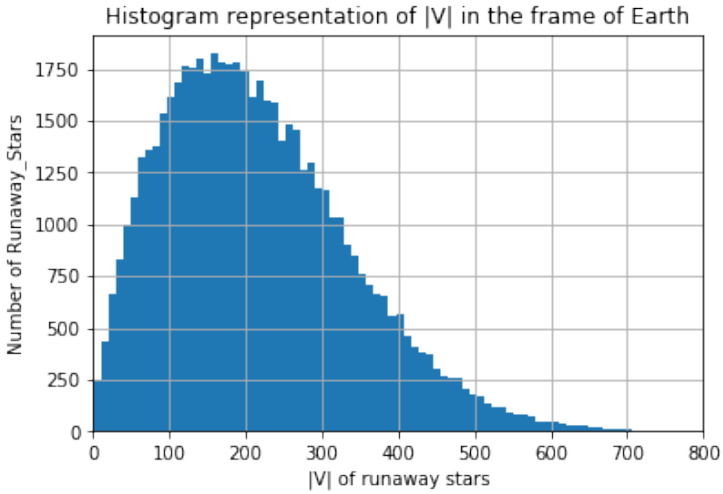

Figure 3.9: Histogram entry of magnitude of velocity projected onto observer's sky.

velocity. First, we randomly orient the binary orbit with respect a virtual observer and we then we project the 3D NS velocity onto the observers plane of the sky. The result for Model 1 is shown in Figure 3.9. For both Models 1 and 2, the projection of the 3D NS velocities does not follow a MB distribution. The histogram entry of the projected velocity shifts to the left of true velocity. We approximated the mode of tangential velocity to be $\sim 150\,\mathrm{km/s}$.

3.3 High Velocity Black Holes

We do not have observational data on high-velocity BHs that we can compare with our results. The numbers on high-velocity black holes are purely speculative. Progenitors of neutron stars and black holes in the binary follow the same stellar evolution process. The asymmetric supernova-kick model that we apply to runaway NSs is also applicable to runaway BHs.

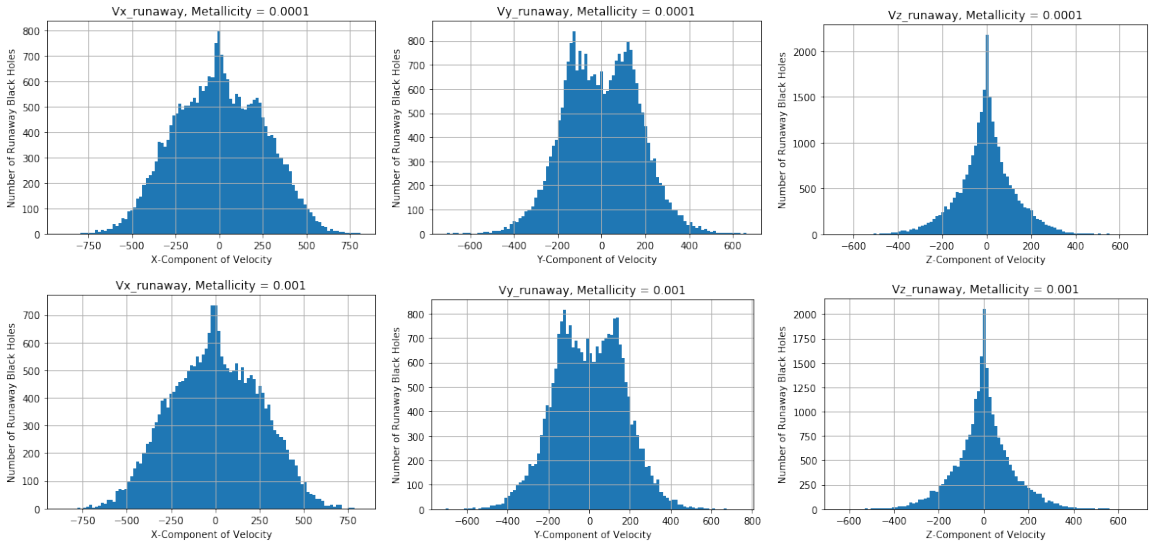

Figure 3.10: X, Y, and Z Components of runaway black holes from left to right for metallicities 0.0001 and 0.001 of Model 1.

The components (X, Y, Z) of the final velocities of runaway BHs in the original frame are identical to the components of NSs in velocity distribution, except for their population (compare Figure 3.3,3.4, 3.10 and 3.11). Just as the components of NSs, the speed is concentrated roughly parallel to the X-Y plane. The direction of the velocity components is symmetrical in all three axes and least favored in the magnitude of the z-axis. It also implies that the spin angle of a spinning BH would have the Z-axis of its progenitor's original plane as its preferential spin axis. The population of runaway BHs in Model 1 is significantly lower than the population of runaway NSs (see Tables 3.1 and 3.2). As listed on the tables, mean, median, and mode are almost identical. Slightly above 5% of runaway BHs exceed 500 km/s for all the metallicities, and roughly 0.07% exceed 750 km/s. Model

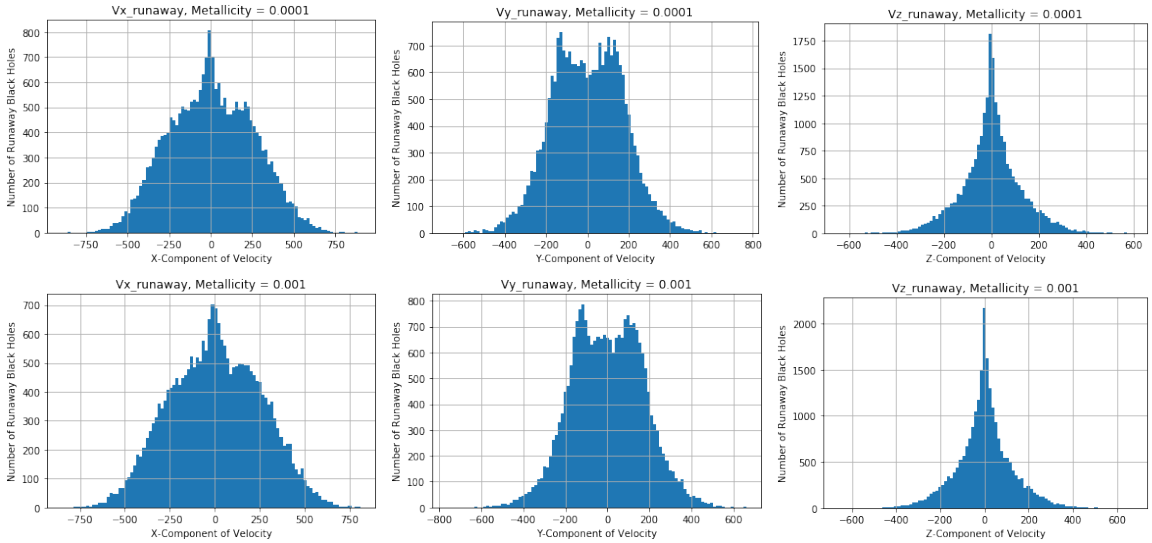

Figure 3.11: X, Y, and Z Components of runaway black holes from left to right for metallicities 0.0001 and 0.001 of Model 2.

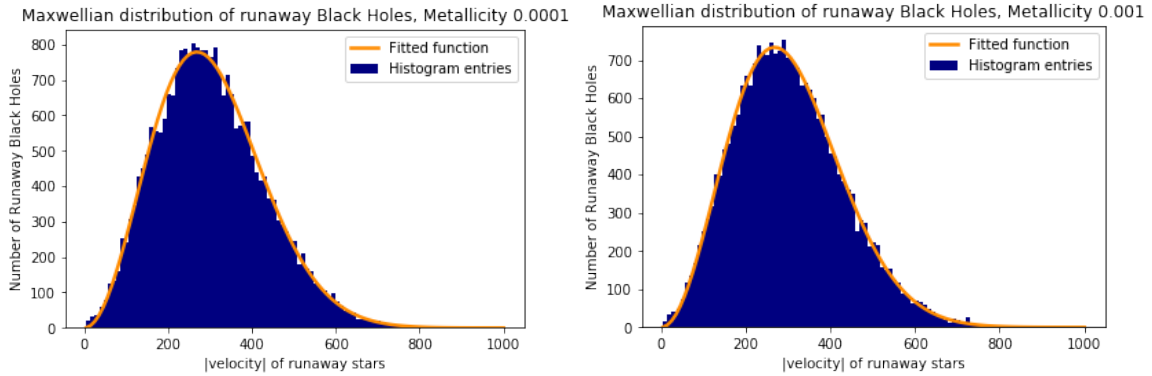

Figure 3.12: Maxwellian distribution of the final velocity of the runaway black holes in the original frame for metallicities 0.0001 and 0.001 of Model 1.

2 generates a slightly lower number of black holes compared to Model 1. Still, the difference in the BH population is not as significant as the difference in population difference of NS in Model 1 versus Model 2. Mean, mode, and median are almost identical to the runaway BH in Model 1. Roughly 5.5% of runaway BH exceed 500 km/s for all the metallicities. Nearly 0.1% of runaway BH exceed 750 km/s. The tight orbital configuration of Model 2 generates a smaller sample of runaway BHs. Still, the average speed of the BHs is roughly the same, which points to one of the consistent conclusions that the SNe-kick dominates the final velocity of a compact object.

Table 3.2: Numerical results from the Velocity Distribution in Maxwellian of the Runaway-BH in an original frame.

Metallicity	Runaway-BH	Mean	Mode	Sigma	>500 km/s	>750 km/s
		km/s	km/s	km/s		
Model 1						
0.0001	25190 ± 158	302	268	127	1393 ± 37	30 ± 5
0.001	23753 ± 154	302	268	127	1264 ± 35	16 ± 4
0.01	19677 ± 140	301	267	127	957 ± 31	16 ± 4
0.02	18906 ± 137	300	266	127	985 ± 31	14 ± 3
Model 2						
0.0001	22956 ± 151	304	269	128	1310 ± 36	24 ± 5
0.001	23823 ± 154	302	267	127	1359 ± 37	22 ± 4
0.01	21662 ± 147	301	268	127	1149 ± 34	20 ± 4
0.02	21238 ± 145	303	269	128	1125 ± 33	24 ± 5

3.4 High Velocity Companions

We call "companions" the stars that are the companion to the NS or BH when these compact objects underwent SN when the binary was disrupted. Their velocity is mostly the orbital velocity they had when they were binaries before the separation.

Compared to Model 2, Model 1 has a very high population of companion stars that obtain non-zero velocity after the binary disruption. The upper period limit of Model 2 is 1500 days, and the stars in the binary system with small orbital period have higher angular momentum compared to stars with a more extended period; companions in Model 1 are concentrated slightly above 5 km/s. Model 2 has a very small population of companions even though the magnitude of the velocity is guaranteed to be higher once the binary is disrupted because of its initial angular momentum.

Xu et al. (2018) studied the runaway velocities of OB stars using velocity data from the GAIA observatory. Based on their study, we have calculated the 3D velocity of these OB stars. The result from the velocity survey of 5700 OB stars, roughly 2500 of them have the

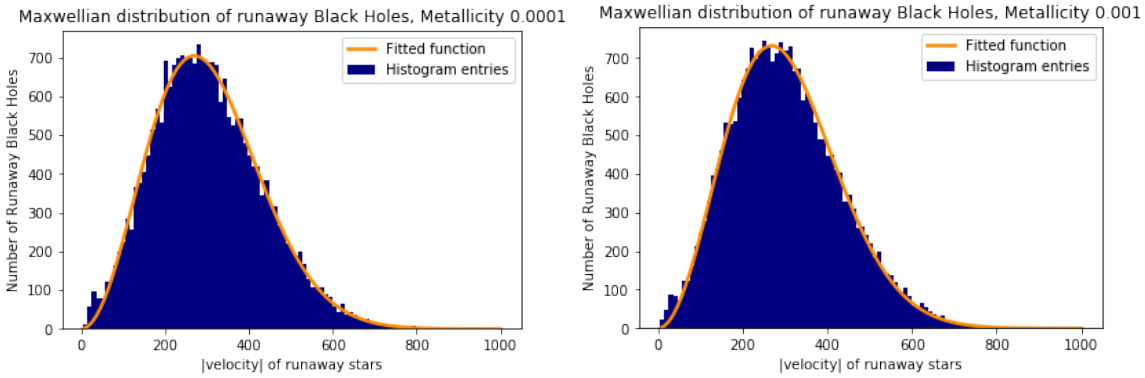

Figure 3.13: Maxwellian distribution of the final velocity of the runaway black holes in the original frame for metallicities 0.0001 and 0.001 of Model 2.

Table 3.3: Numerical results of the Companions' Velocity in an original frame for the Model 1

Metallicity	Companions	>20 km/s	>50 km/s
Model 1			
0.0001	35762 ± 189	5130 ± 71	629 ± 25
0.001	33068 ± 182	4008 ± 63	715 ± 26
0.01	27530 ± 166	2093 ± 45	345 ± 18
0.02	26158 ± 161	1317 ± 36	184 ± 13
Model 2			
0.0001	4020 ± 63	2460 ± 50	308 ± 17
0.001	3360 ± 58	1682 ± 41	232 ± 15
0.01	2534 ± 50	595 ± 24	84 ± 9
0.02	2344 ± 48	514 ± 22	57 ± 7

Table 3.4: OB stars velocity data from GAIA survey

OB Stars>0 Km/s	>20 km/s	>50 km/s
2557 ± 50	1975 ± 44	1032 ± 32

true velocity > 0 km/s. Histogram (Figure 3.14) shows the velocity is concentrated roughly at 20 km/s. Roughly 1975 (77%) exceed 20 km/s and 1032 (40%) exceed 50 km/s. Our numerical simulation for Model 2 generates the sample (Table 3.3) with 61.2%, 50.1%, 23.9%, and 21.9% for metallicities 0.0001, 0.001, 0.01, and 0.02 respectively. We find metallicity 0.0001 of Model 2 to be the closest match to the observed sample (Table 3.4).

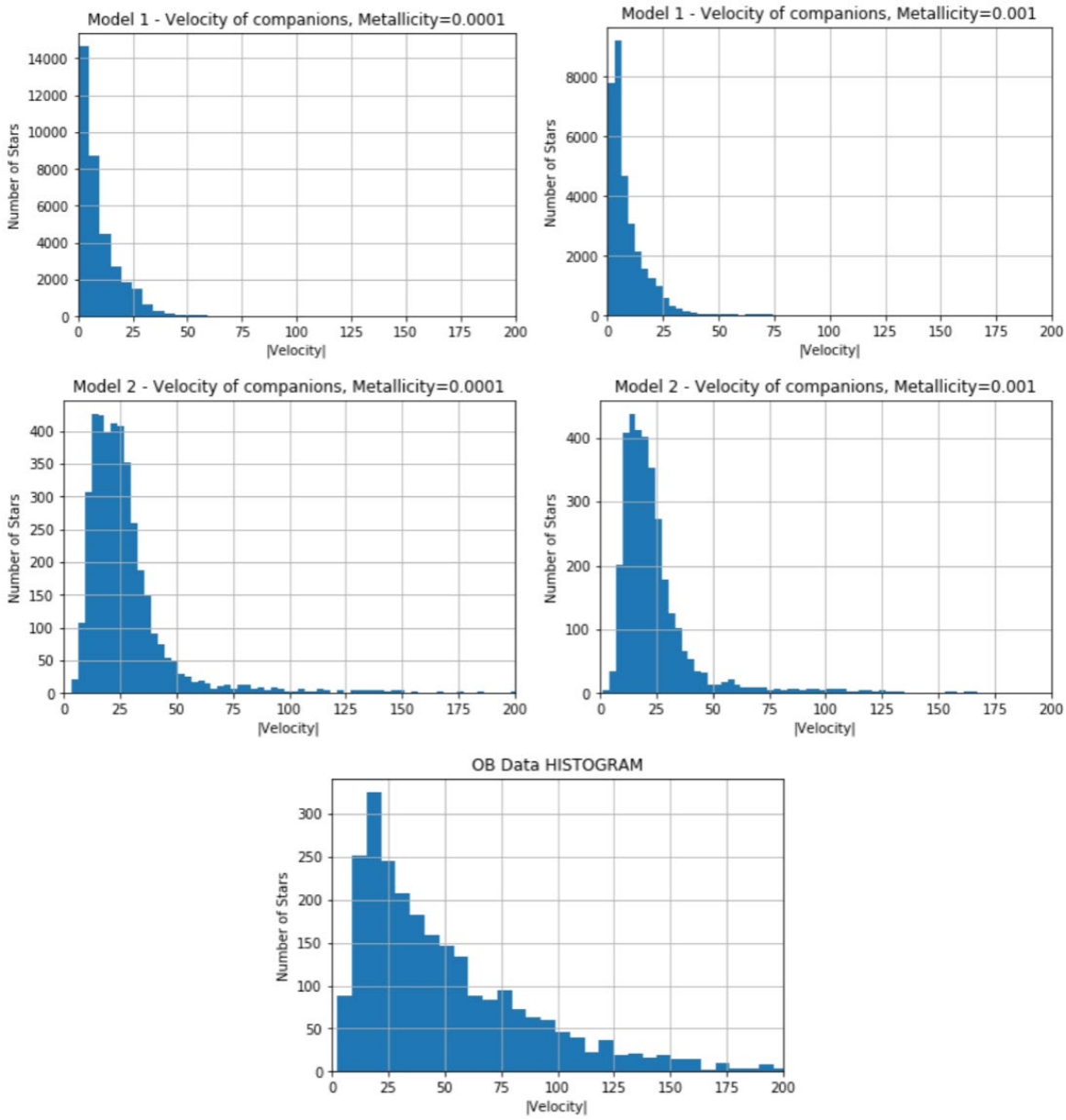

Figure 3.14: Histogram representation of velocity of companions (top 4 histograms), and histogram representation of velocity of stars from GAIA survey (bottom).

4. CONCLUSION AND FURTHER RESEARCH

4.1 Conclusion

We have presented a numerical simulation of different binary states in the aftermath of a SN and runaway stars originating from the binary system. Observational data are rare, and we only have very small samples of catalogs on runaway pulsars. We have offered statistical insights with substantial data on runaway NSs and speculative data on runaway BHs. We ran two different models of initial binary parameters, and we explored different metallicities for each model. The binary parameters for Model 1 were adopted from Kroupa et al. (1993); Sana et al. (2012).

NS-Companion binary is the most significant fraction that remains binary. In contrast, the BH-BH binary is the least likely state for both models. We found that the SN kick dominates the final velocity of the runaway stars. The kick imparted during the SNe follows the MB distribution. The final 3-D velocity also follows the MB distribution because the angular velocity has little to no effect on the final velocity. The mean of the final velocity peaks slightly above 300 km/s, which is also roughly the mean of the SN-kick. While our simulations show similar distributions for runaway NS velocities, the distribution parameters slightly differ from the observations. This is likely due to complexity of initial velocities of binaries from their birth places and their location within the Galaxy with respect to Earth.

Another potentially interesting application of our simulations is with respect to origin of diversity of shapes among PWNe. We found that the spin axis of runaway NSs is usually perpendicular to their motion. This suggest that the tails behind pulsars may be due to bent jets. Nevertheless, the strength of the pulsar wind still pays very important role. If the pulsar wind is still very powerful (typically for young pulsars), this could explain why

some PWNe are “filled” with emission rather than to “empty”. While we cannot predict the shapes of all PWNe based on our simulation, we hope we can explain the origins of some PWNe.

We have also looked at the velocity of massive stars after the binary disruption and compared the simulations with the GAIA data. While we do not find a perfect fit, we found that Model 2 (tighter binary setup) with metallicity of 0.0001 matches best the observed velocity distribution of OB stars.

4.2 Further Research

- When stars (and binaries) form, they are not born in a stationary environment. Just as the Sun rotates around the center of the Galaxy, so do star forming regions and young stars. To make are simulations more realistic, we will randomly “place” our simulated binaries along the Galactic spiral arms and calculate their perceived 2-D and 3-D velocities as they appear from Earth. This may help obtain more realistic results for the pulsar velocity distributions. We will also explore how changing the intrinsic SN-kick velocity distribution can affect the final results.
- Explore the more binary parameters, e.g., models, which may result in different outcomes.
- Looking into the formation of X-ray binaries is another interesting application of our methods, which was beyond the scope of this study.
- We will calculate the ratio of SNRs we expect to have binary residing within the remnant, and those for which a compact source is expected. This will be directly comparable with observations.
- We will look at observational results of PWNe, which have tails trailing behind, and those with confidently identified jets.
- A limitation of our simulations is that we evolve the binaries in isolation. We know

that most stars form in groups or clusters of stars. We will explore how the cluster environments can affect of binary evolution. We will achieve this by running the `Nbody6` code, which simulates the stellar interactions in a star cluster. The `Nbody6` calculates the gravitational forces directly, it is a lot more computationally intensive than `binary_c`, and it will require significant time to run even a modest population of stars.

M. J. Benacquista. *An Introduction to the Evolution of Single and Binary Stars*, volume 1 of *1*. Springer-Verlag New York, 1st edition, Aug. 2013. ISBN 978.

A. P. Boss. Protostellar Formation in Rotating Interstellar Clouds. VII. Opacity and Fragmentation. , 331:370, Aug. 1988. doi: 10.1086/166563.

Casares, Martínez-Pais, and Rodríguez-Gil. SY Cnc, a case for unstable mass transfer? *Monthly Notices of the Royal Astronomical Society*, 399(3):1534–1538, 10 2009. ISSN 0035-8711. doi: 10.1111/j.1365-2966.2009.15384.x. URL https://doi.org/10.1111/j.1365-2966.2009.15384.x.

B. Dincel, R. Neuhäuser, S. K. Yerli, A. Ankay, N. Tetzlaff, G. Torres, and M. Mugrauer. Discovery of an OB runaway star inside SNR S147. *Monthly Notices of the Royal Astronomical Society*, 448(4):3196–3205, 03 2015. ISSN 0035-8711. doi: 10.1093/mnras/stv124. URL https://doi.org/10.1093/mnras/stv124.

P. L. Dufton, P. R. Dunstall, C. J. Evans, I. Brott, M. Cantiello, A. de Koter, S. E. de Mink, M. Fraser, V. Hénault-Brunet, I. D. Howarth, N. Langer, D. J. Lennon, N. Markova, H. Sana, and W. D. Taylor. The VLT-FLAMES Tarantula Survey: The Fastest Rotating O-type Star and Shortest Period LMC Pulsar—Remnants of a Supernova Disrupted Binary? , 743(1):L22, Dec. 2011. doi: 10.1088/2041-8205/743/1/L22.

G. Fabbiano. Populations of X-Ray Sources in Galaxies. , 44(1):323–366, Sept. 2006. doi: 10.1146/annurev.astro.44.051905.092519.

G. Hobbs, D. R. Lorimer, A. G. Lyne, and M. Kramer. A statistical study of 233 pulsar proper motions. , 360(3):974–992, July 2005. doi: 10.1111/j.1365-2966.2005.09087.x.

T. Holland-Ashford, L. A. Lopez, K. Auchettl, T. Temim, and E. Ramirez-Ruiz. Comparing Neutron Star Kicks to Supernova Remnant Asymmetries. , 844(1):84, July 2017. doi: 10.3847/1538-4357/aa7a5c.

J. R. Hurley. Nuclear and dynamical evolution of stellar systems. *The Observatory*, 120: 426–427, Dec. 2000.

R. G. Izzard. Duplicitous Nucleosynthesis. , 75:754, Jan. 2004.

R. G. Izzard, L. M. Dray, A. I. Karakas, M. Lugaro, and C. A. Tout. Population nucleosynthesis in single and binary stars. I. Model. , 460(2):565–572, Dec. 2006. doi: 10.1051/0004-6361:20066129.

P. C. Joss. Type II Supernovae in Binary Systems. In J. van Paradijs, E. P. J. van den Heuvel, and E. Kuulkers, editors, *Compact Stars in Binaries*, volume 165, page 141, Jan. 1996.

O. Kargaltsev and G. G. Pavlov. Pulsar Wind Nebulae in the Chandra Era. In C. Bassa, Z. Wang, A. Cumming, and V. M. Kaspi, editors, *40 Years of Pulsars: Millisecond Pulsars, Magnetars and More*, volume 983 of *American Institute of Physics Conference Series*, pages 171–185, Feb. 2008. doi: 10.1063/1.2900138.

M. B. N. Kouwenhoven, A. G. A. Brown, S. P. Goodwin, S. F. Portegies Zwart, and L. Kaper. Exploring the consequences of pairing algorithms for binary stars. , 493(3): 979–1016, Jan. 2009. doi: 10.1051/0004-6361:200810234.

P. Kroupa, C. A. Tout, and G. Gilmore. The Distribution of Low-Mass Stars in the Galactic Disc. , 262:545–587, June 1993. doi: 10.1093/mnras/262.3.545.

R. B. Larson. The physics of star formation. *Reports on Progress in Physics*, 66(10):1651–1697, Oct. 2003. doi: 10.1088/0034-4885/66/10/R03.

J. M. Lattimer and M. Prakash. The physics of neutron stars. *Science*, 304:536–542, 2004. doi: 10.1126/science.1090720.

A. G. Lyne and D. R. Lorimer. High birth velocities of radio pulsars. , 369(6476):127–129, May 1994. doi: 10.1038/369127a0.

O. Malkov and D. Chulkov. Catalogues, parameters and distributions of orbital binaries. 04 2017.

N. I. Maxted, A. J. Ruiter, K. Belczynski, I. R. Seitenzahl, and R. M. Crocker. A supernova remnant associated with a nascent black hole low-mass X-ray binary. *arXiv e-prints*, art. arXiv:2010.15341, Oct. 2020.

V. Niemela. A Short History and Other Stories of Binary Stars. In *Revista Mexicana de Astronomia y Astrofisica Conference Series*, volume 11 of *Revista Mexicana de Astronomia y Astrofisica Conference Series*, pages 23–26, July 2001.

O. Pols, J. Hurley, and C. Tout. An efficient evolution algorithm for population synthesis of AGB stars. *IAU Symposium*, 191:P607, Jan. 1998.

A. H. Prestwich, J. A. Irwin, R. E. Kilgard, M. I. Krauss, A. Zezas, F. Primini, P. Kaaret, and B. Boroson. Classifying X-Ray Sources in External Galaxies from X-Ray Colors. , 595(2):719–726, Oct. 2003. doi: 10.1086/377366.

B. Rangelov, A. H. Prestwich, and R. Chandar. The Connection between X-Ray Binaries and Star Clusters in NGC 4449. , 741(2):86, Nov. 2011. doi: 10.1088/0004-637X/741/2/86.

B. Rangelov, R. Chandar, A. Prestwich, and B. C. Whitmore. X-Ray Binaries and Star Clusters in the Antennae: Optical Cluster Counterparts. , 758(2):99, Oct. 2012. doi: 10.1088/0004-637X/758/2/99.

H. Sana, S. E. de Mink, A. de Koter, N. Langer, C. J. Evans, M. Gieles, E. Gosset, R. G. Izzard, J. B. Le Bouquin, and F. R. N. Schneider. Binary Interaction Dominates the Evolution of Massive Stars. *Science*, 337(6093):444, July 2012. doi: 10.1126/science.1223344.

F. H. Shu. Ambipolar diffusion in self-gravitating isothermal layers. , 273:202–213, Oct. 1983. doi: 10.1086/161359.

F. H. Shu, F. C. Adams, and S. Lizano. Star formation in molecular clouds: observation and theory. , 25:23–81, Jan. 1987. doi: 10.1146/annurev.aa.25.090187.000323.

J. Southworth. Eclipsing Binary Stars: the Royal Road to Stellar Astrophysics. 1 2012.

O. Struve and S. S. Huang. *Spectroscopic Binaries*, pages 243–273. Springer Berlin Heidelberg, Berlin, Heidelberg, 1958. ISBN 978-3-642-45906-1. doi: 10.1007/978-3-642-45906-1_8. URL https://doi.org/10.1007/978-3-642-45906-1_8.

T. M. Tauris and R. J. Takens. Runaway velocities of stellar components originating from disrupted binaries via asymmetric supernova explosions. , 330:1047–1059, Feb. 1998.

N. Tetzlaff, B. Dinçel, R. Neuhäuser, and V. V. Kovtyukh. The origin of the young pulsar PSR J0826+2637 and its possible former companion HIP 13962. , 438(4):3587–3593, Mar. 2014. doi: 10.1093/mnras/stt2478.

M. Zhao, D. Gies, J. D. Monnier, N. Thureau, E. Pedretti, F. Baron, A. Merand, T. ten Brummelaar, H. McAlister, S. T. Ridgway, N. Turner, J. Sturmann, L. Sturmann, C. Farrington, and P. J. Goldfinger. First Resolved Images of the Eclipsing and Interacting Binary β Lyrae. , 684(2):L95, Sept. 2008. doi: 10.1086/592146.